International Journal of Heat and Mass Transfer 138 (2019) 390–400

Contents lists available at ScienceDirect

International Journal of Heat and Mass Transfer

journal homepage: www.elsevier.com/locate/ijhmt

Experimental study on convective boiling of micro-pin-finned channels with parallel arrangement fins for FC-72 dielectric fluid

Liang-Han Chien [a,b], Wun-Rong Liao [c], Mohammad Ghalambaz [d,e], Wei-Mon Yan [a,b,*]

[a] Department of Energy and Refrigerating Air-Conditioning Engineering, National Taipei University of Technology, Taipei 10608, Taiwan
[b] Research Center of Energy Conservation for New Generation of Residential, Commercial, and Industrial Sectors, National Taipei University of Technology, Taipei 10608, Taiwan
[c] National Synchrontron Radiation Research Center, Hsin-Chu, Taiwan
[d] Department for Management of Science and Technology Development, Ton Duc Thang University, Ho Chi Minh City, Viet Nam
[e] Faculty of Applied Sciences, Ton Duc Thang University, Ho Chi Minh City, Viet Nam

ARTICLE INFO

Article history:
Received 6 October 2018
Received in revised form 9 April 2019
Accepted 14 April 2019
Available online 19 April 2019

Keywords:
Microchannel
Flow boiling
Parallel nucleate micro-pin-fin
Dielectric fluid

ABSTRACT

The boiling convective heat transfer of dielectric fluid of FC-72 in a microchannel with etched micro fins is experimentally studied. The microchannel test surface is a square of 10 mm size with a height of 100 μm. The surface of the microchannel is covered with parallel-nucleated fins of a cubic size of 100 μm. The fins are nucleated with the central pore size of 60 μm and an opening of 45 μm. The fins are arranged in the equal space of 400 μm. There is a planar electrical element below the microchannel, which produces an adjustable surface heat flux below the channel. The dielectric liquid enters the test microchannel and flows over the test surface and the fins. In the experiments, the mass velocity (94–275 kg/m^2 s) and heat flux (0–6 W/cm^2) are tested with a saturation temperature of either 35 or 50 °C. The heat transfer, the outlet vapor quality, and the pressure drop across the microchannel are measured and reported. The boiling behavior of FC-72 over the etched fins is also investigated using photos. The results show that the liquid first go through some superheat states and then the boiling phase change starts. When the boiling heat transfer occurs, a significant pressure-drop can be observed across the microchannel, but the surface temperature difference would also drop significantly. In the case of very low mass velocity of 94 kg/m^2 s, the minimum superheat temperature-difference of 4.7 °C is observed.

1. Introduction

With the advancement of technology, new generations of electronic products continue to evolve, and the heat density of computer-based chips has increased. Therefore, there is a continues increasing demand for high-efficiency cooling systems. One-way to cooling of electronic products is the liquid cooling. In the liquid cooling mechanism, the liquid coolant absorbs the generated heat of the electronic components through some heat sinks by the liquid convection, and then, the liquid flows away and dissipate the heat to surrounding through air-cooled radiators. Reviewing the development of high heat-flux cooling system technologies in recent years shows that the liquid cooling mechanisms such as multiple microchannels radiators, micro gap radiators, pressurizing liquids with nozzle sprays on the hot surface, jet impingement and sprays are the cooling mechanisms with development potentials [1].

As an example of high demand cooling systems, in 2008, International Business Machines Corporation (IBM) released a server Power 575 [2], consisting of 16 dual-core systems running at 4.7 GHz per chip and with 3.5 TB of random memory. A liquid cooling heat dissipation system was adopted to improve the heat transfer performance and reduce the thermal impedance of the system. The analysis of this liquid cooling system reveals that the power consumption of the liquid-cooled cooling system is 45% lower than that of the conventional air-conditioning system [3].

Alfieri et al. [4] proposed a micro-sized stacked heat sink, manufactured using three-dimensional wafer fabrication technology, to achieve the goal of low-pressure loss and high heat dissipation rate. They applied this technology to the heat recovery of the heat dissipation of the chip and applied it to the air conditioning heating of the IBM computer room to achieve the low carbon energy saving goal of the computer room operation. The results show that a heat flux of 250 W/cm^2 can be achieved with this ultra-small heat sink when the cooling fluid is water.

* Corresponding author at: Department of Energy and Refrigerating Air-Conditioning Engineering, National Taipei University of Technology, Taipei 10608, Taiwan.
E-mail address: wmyan@ntut.edu.tw (W.-M. Yan).

https://doi.org/10.1016/j.ijheatmasstransfer.2019.04.072
0017-9310/

Nomenclature

A_c	cross-sectional area of the microchannel (m^2)
A_p	projected area (m^2)
C_p	specific heat capacity of the fluid (J/kg °C)
f	function
G	mass velocity (kg/m^2 s)
h_{fg}	the enthalpy of phase change from liquid to vapor (J/kg)
k	thermal conductivity of the microchannel
k_f	thermal conductivity of the fluid (W/m °C)
$\dot{m}$	the mass flow rate (kg/s)
P	pressure (Pa)
P_i	Inlet pressure of the test section (kPa)
P_o	Outlet pressure of the test section (kPa)
Q	input power (W)
q''	surface heat flux (W/m^2 K)
Q_{loss}	heat loss (W)
T	temperature (°C)
T_{in}	inlet temperature of the fluid (°C)
T_{sat}	saturation temperature of the fluid (°C)
T_w	test surface wall temperature (°C)
V	input voltage (V)

Greek symbol

μ	dynamic viscosity (Pa × s)
ρ_f	fluid density (kg/m^3)
ρ_g	gas density (kg/m^3)
σ	surface tension coefficient (N/m)

The type of convection heat-dissipation mechanisms can be divided into single-phase and two-phase convection [5]. The difference in heat transfer performance is mainly affected by the sensible heat and latent heat mechanism. In the two-phase heat transfer mechanism, the heat is taken away by latent heat, so that higher heat transfer performance can be obtained. Another advantage of two-phase heat transfer mechanism is the requirement of a low amount of working fluid. Considering two-phase heat transfer mechanisms, the pool boiling phase change is an efficient cooling method. However, it is not sufficient for computer and high-power electronic cooling. In practice, the heat generation in computer components changes suddenly from low to high. The convection would also change from the natural convection to boiling convection. However, the main drawback of pool boiling cooling system is the boiling initial superheat temperature (incipient superheat) which is too high.

In contrast, in the "forced convection boiling" cooling mode, when boiling has not yet occurred, there is a forced convection cooling mechanism in which the fluid flows through the microchannel with a high heat transfer coefficient. The initial superheat boiling in microchannels may be reduced by using some fins. As the fins improve heat transfer performance, so the forced-convection boiling heat-dissipation mode could be a highly feasible computer-cooling mode.

Lie et al. [6] fabricated a micro-fin structure on the surface of a wafer with a channel height of 5 mm, fins dimensions of 200 μm × 200 μm × 70 μm and 100 μm × 100 μm × 70 μm (width × length × height). The fin spacing was considered as equal to the width of the fin, and the working fluid was adopted as FC-72. The experimental results show that placing the micro fins in a microchannel will increase the single relative flow and the two-phase boiling heat transfer coefficient. The fins reduce the bubble detachment diameter and increase the bubble detachment frequency. The fins also increase the number of bubble nucleation boiling points at higher heat fluxes.

Ye and Yang [7] have used a micro-product process to produce a micro-channel heat dissipation mechanism with a length and width of 50 mm and a thickness of 2 mm. The micro-channel type includes a mountain pattern, an intermittent pattern, a wing shape, a shuttle shape, and traditional flat shape. The working fluid was water which its temperature in the inlet was controlled at 30 °C, the flow rate was set to 50–250 ml/min, the heating power was 20–100 W, and then the performance of different channel surfaces was explored. The research results show that the mountain pattern channel produces higher disturbance effect, so the surface temperature is uniform and low. In this case, the overall heat transfer performance is the best, but higher pump power is required, and higher pressure-loss is generated. They also reported that the heat transfer performance of the continuation channel is slightly lower than that of the mountain pattern, but the relative pressure-drop is small.

Escher et al. [8,9] fabricated a microchannel structure fin similar to a multi-porous staggered stack after deep etching of a tantalum wafer. The cooling fluid enters the microchannel through a layer underside of the channel. The micro-channels were arranged to produce a hybrid porous spray and multi-layer micro-channels. The projected surface area of the heat-dissipating surface was 2 × 2 $cm^{2,}$ and the height was less than 2 mm. The number of micro-channels was explored by experiment and semi-empirical simulation. The channel aspect ratio and microchannel wall thickness were analyzed for heat transfer performance, convection thermal resistance, and pressure drop. The research results show that the cooling fluid can generate three-dimensional flow field in this mechanism and effectively suppressing the temperature layer development of the channel. When the number of microchannels in below layer of the wafer reduces, the fluid thermal resistance and pressure-drop of the whole system will increase significantly. The increase in the flow rate of the cooling fluid reduces the thermal resistance of the fluid.

Considering the boiling heat transfer in a channel over obstacles, Hwang and Yao [10], Hsu [11], Jensen and Hsu [12], Gupta et al. [13] and Gupta [14] have studied the boiling flow heat transfer in tube bundles. Very recently, different aspects of flow and heat transfer in microchannels have been investigated. In this regard, the microfluidic effects [15], film condensation flow [16], binary thin liquid film [17], flow boiling of FC-72 in backward and forward facing stepped microchannels [18], thermal creep flow in a thin microchannel [19], slug flow boiling in square microchannels [20], pool boiling heat transfer with segmented finned microchannels structured surface [21], high aspect-ratio microchannels [22], critical heat flux of flow boiling in parallel microchannels [23], flow and heat transfer of oil-in-water emulsions [24], ribbed microchannel [25], twisted sinusoidal wavy microchannels [26] have been addressed.

Wei and Joshi [27] have used numerical simulation to investigate the pressure-drop and heat transfer performance of a five-layer stacked rectangular flow path. The research results show that when the pressure-drop of the stacked flow channel is fixed, the thermal resistance decreases as the number of stacked layers increases. Moreover, when the flow rate is fixed, the thermal resistance is inversely proportional to the number of stacked layers of the flow channel in the upper two layers. However, when the fluid

passes through the third layer passages, the thermal resistance increases as the number of layers of the flow channel stack increases. Later, Wei et al. [28] used a deep etching and anodic bonding technique to produce a five-layer stacked microchannel with an appearance of 20 mm long, 16 mm wide and 2 mm high. Hsieh and Lin [29] have used PDMS material process technology to make microchannels with a length of 30,000 μm and a width of 200 μm and a depth of 100 μm. The triangular pores were formed on both sides of the wall, and 200 pores were opened on each side. The opening area of the pores was 100 μm × 50 μm. The hole angles were 0°, 60°, 90° and 120°. The working fluid was water and FC-72. Experimental observations show that the channels with vent holes are more effective in enhancing the heat transfer performance and reducing the degree of overheating required for initial boiling.

Novianto et al. [30] have addressed the single-phase flow near the boiling heat transfer of propane in a horizontal circular microchannel with a diameter of 500 μm. The test-section inlet temperature was 21–26 °C. It is found that Reynolds and Prandtl numbers notably affect the convective heat transfer coefficient.

Korniliou et al. [31] studied the local wall temperature maps of flow boiling heat transfer of FC-72 in a transparent microchannel using high frequency and high spatial resolution infrared thermography. Using a high-speed thermography and flow visualization was provided detailed information for two-phase flow and bubble dynamics in the channel. Mathew et al. [32] pointed out that a stable flow boiling process is key to improving the two-phase cooling performance of microchannel heat sinks. They proposed an innovative copper heatsink composed of a straight microchannel array in the upstream region and a microgap channel in the downstream region of the flow boiling. They conducted experiments for water as the working fluid with the inlet temperature of 85.5 °C. The outcomes show that the presence of a microgap at the downstream enhances the flow boiling and increases the boiling stability.

Yin et al. [33] proposed an open microchannel for flow boiling heat transfer. The geometry of the study is similar to a microgap with the etched long-fins perpendicular to the flow stream. The etched fins partially fill the gap space. The water as the working fluid enters the microgap and flows over the fins forming an open microchannel. The effect of different fin geometries was studied. The outcomes show that increasing the number of fins (reducing the size of open channels) enhances the heat dissipation rate but also increases the pressure drop in stratified flow regimes.

Lee et al. [34] have studied large length-to-diameter two-phase microchannel heat sinks for application in future space vehicles. They employed R134a as the working fluid. Parahovnik et al. [35] have addressed the convective boiling in a microchannel with a streamlined pin fin obstacle. Yu et al. [36] have investigated the subcooled flow boiling heat transfer in a microchannel enhanced with Piranha pin fins. They employed HFE-7000 as the working fluid. They performed experiments for mass velocities in the range of 618 kg/m^2 s to 2569 kg/m^2 s, and they achieved the heat fluxes up to 735 W/cm^2. The results show that using the pin fins significantly enhances the flow boiling heat transfer. Woodcock et al. [37] have also utilized the Piranha pin fins in a microgap for ultra-high heat flux dissipation and studied the two-phase cooling performance of HFE-7000 in the microgap. They demonstrated that the heat dissipation rate could exceed 1000 W/cm^2. Kim and Mudawar [38] have discussed the thermal design and operational limits of micro-channel heat sinks for two-phase boiling convective heat transfer. They reported a parametric study for R134a, water and HFE-7100. Kim and Mudawar have discussed the operational limits of two-phase micro-channel heat sinks.

The literature review shows that there is no study to address the convective boiling in the microchannel with nucleated fins. The present work aims to study the flow and boiling convection heat transfer of FC-72 liquid dielectric in a microchannel with a nucleated fin in a parallel array for the first time. The surface temperature, vapor quality, and boiling pressure-drop are studied. The boiling flow patterns are discussed.

2. Experimental

In this research, the forced-convection boiling-heat-transfer performance and the pressure loss in a microchannel are experimentally studied. The cold working liquid continuously flows through the test surface 10 × 10 mm^2 microchannel. The working fluid operates in a closed loop system, and the forced convection boiling occurs in a microchannel test module. An external circulation pumping system is utilized to pressurize the working fluid and sent it to the microchannel. The schematic diagram of the forced convection boiling test system is depicted in Fig. 1. The test system can be roughly divided into a working fluid circulation system, simulated wafer heating system, liquid storage and filtration system, condensation circulation system, filling and degassing system and image capture the system. The details of each section are described in the following sections.

2.1. Working fluid circulation system

The working fluid in a closed loop passes through components in the system circulation line, including a micro gear-pump, a flow meter, a filter, a temperature control system, the microchannel, and a liquid storage tank. FC-72 is adopted as the working fluid in the present experiment. The micro gear-pump drives the fluid to a float-type flowmeter, where the flowmeter measures the flow rate required by the experiment. The working fluid then passes through a filter to remove the tiny particles. The filter is required as the very tiny microparticles can block the microchannel passages. After the filter, there is a temperature control system to control the temperature of the fluid entering the inlet of the microchannel, which guides the coolant liquid to the microchannel heatsink in the test area. The working fluid in the microchannel is partially evaporated into a gaseous form. Hence, when the liquid flows through the column-shaped microchannel of the test area to go through a phase change, the liquid and gases will be sucked through the outlet of the microchannel to be taken away from the microchannel. Later, the gaseous working fluid will be condensed into a liquid via a condenser and stored in the bottom of the condenser. Finally, the collected working fluid is filtered through a filter and returned to the micro gear-pump, and a new cycle commenced. Three T-type thermocouples are installed in front of the test area to measure the temperature of the working fluid. One is placed in the fluid line, and the other two are attached to the tube wall. An electronic pressure gauge is placed at the entrance. The inlet pressure is measured to estimate the saturation temperature of the inlet to indicate the inlet sub-cooling degree. An electronic differential pressure gauge is provided between the liquid inlet and the outlet to measure the pressure difference induced by the liquid passing through the test area. The working range of the differential pressure gauge is 0–150 kPa.

2.2. Analog wafer cooling system

The schematic diagram of the experimental test module is depicted in Fig. 2. The test module consists of a flow-guiding basis, a heating source, a test wafer, and a heat-insulating layer. As shown in Fig. 2, a 2 mm thick asbestos gasket with a 1 mm Teflon gasket layer are employed as the insulation substrate for the film heater. The thin heater powers up using an AC power source. The

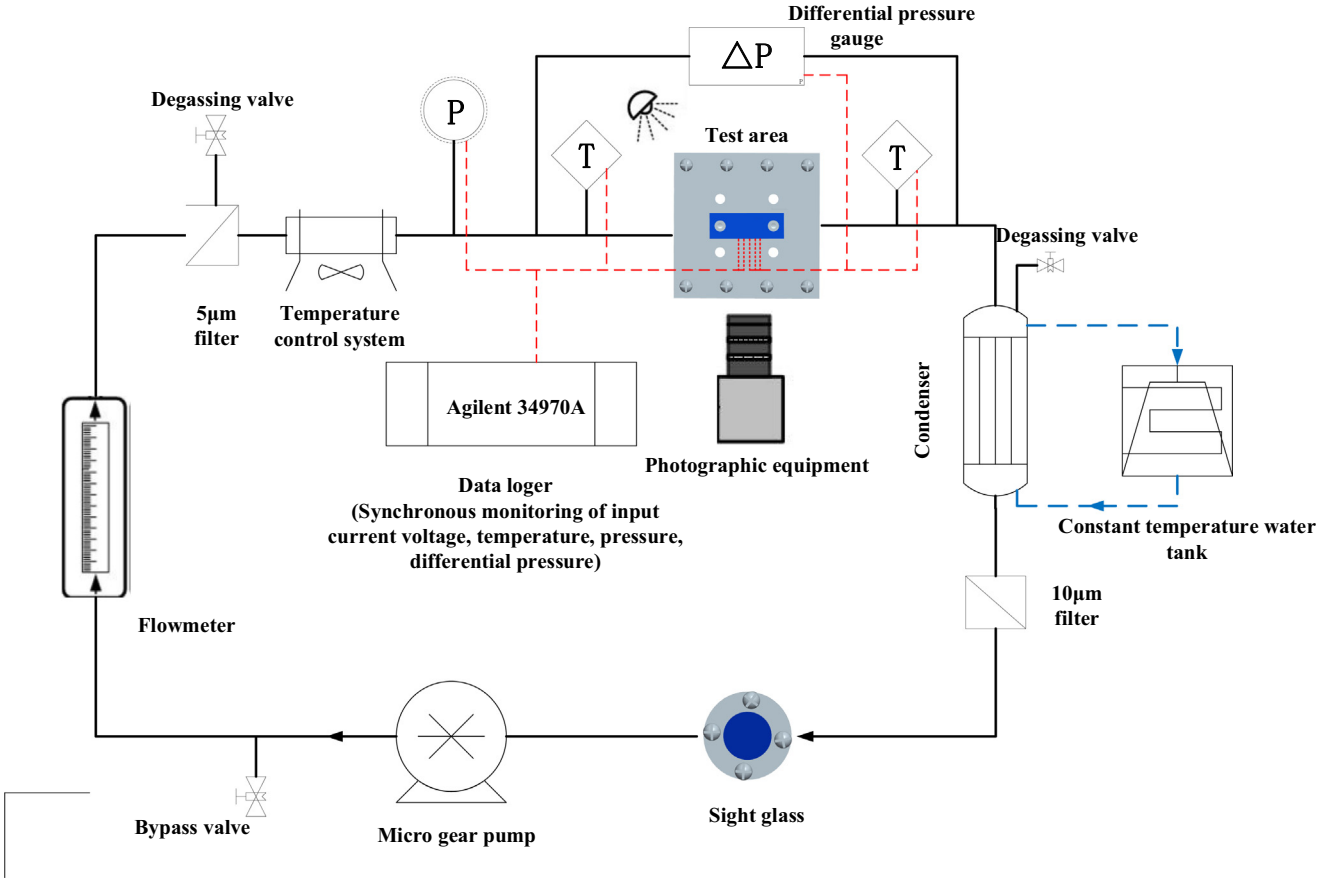

Fig. 1. Schematic view diagram of the forced convection boiling system.

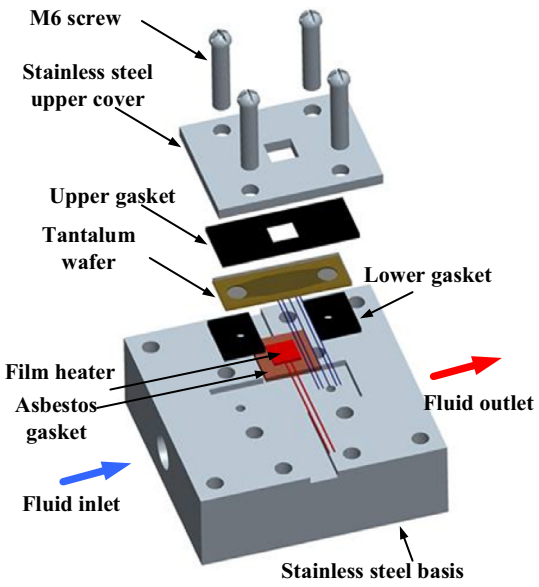

Fig. 2. Schematic view of the test module.

insulation layer thermally disconnects the film heater and the heating zone from the stainless-steel basis. A Teflon gasket layer prevents the gaseous FC-72 from reaching to the film heater and the asbestos layer. The asbestos gasket with the size of $16 \times 20\ mm^2$ provides large enough area for the placement of the thin film heater with a size of $10 \times 10 \times 0.5\ mm^3$. A tantalum wafer with the test surface size of $16 \times 46 \times 1.7\ mm^3$ is placed over the asbestos and Teflon insulation layers. The backside of the wafer is engraved with five grooves. T-type thermocouples are used to measure the temperature of the wafer. A 2 mm thick rubber gasket is utilized at the wafer inlet and outlet to prevent the liquid leakage effect at the joints. A 3 mm thick stainless-steel piece is used as the upper clamp cover. A $10 \times 10\ mm^2$ cut is made at the center of the stainless-steel cover as a window for the test surface observation. A 2 mm thick rubber gasket is placed between the stainless-steel cover and the test wafer for uniform heat and force application. The film heater and wafer are locked and fixed on the flow guiding stainless-steel basis by four M6 stainless-steel screws. The center of the stainless-steel basis is carved in a cavity with the size of $18 \times 48 \times 3\ mm^3$ to provide a fixed place for mounting of the test wafer and film heater. The front inlet and rear outlet of the stainless-steel basis are connected to the copper pipelines. The working fluid enters the basis and will be introduced into the test wafer through a small channel passage in the basis. The working fluid passes through the wafer and exits the wafer through a small machined channel to the basis outlet. By using eight M6 stainless-steel screws, the stainless-steel basis is fixed on a shockproof table convenient for experimental observations. Finally, the overall wafer heat-dissipation system is coated with insulation cotton to prevent heat loss.

2.3. Test surface

The test surface of this experiment is a 46 mm long × 16 mm wide × 0.5 mm high rectangular wafer. The photo of the test surface is depicted in Fig. 3(a). The microchannels with a depth of 100 μm were etched on the surface, including the inlet, the conver-

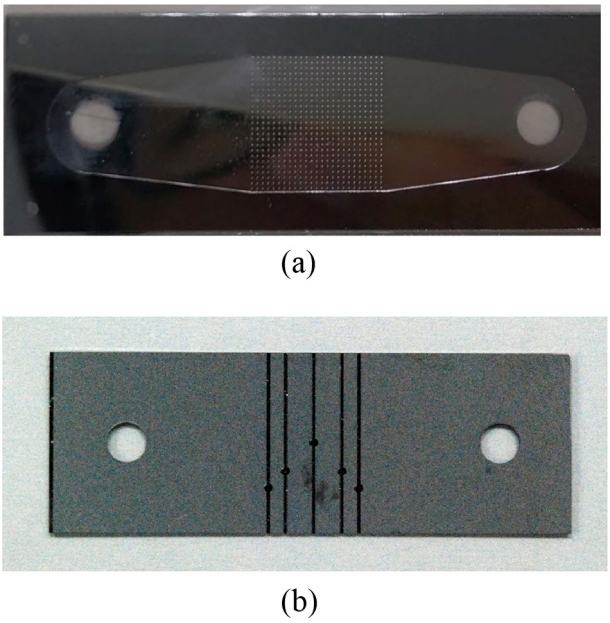

Fig. 3. The photograph of the test wafer after drilling, (a) front side of the wafer (including test surface), (b) back side of the wafer (including thermocouple channel).

gent area, the test surface, the divergent area, and the outlet. Five temperature measurement points are processed in the range of 10 mm × 10 mm. The measurement point size is 80 μm and 170 μm deep to accommodate the thermocouple. A photo of the temperature measurement points and the wiring channels are depicted in Fig. 3(b). Over the test surface area, 613 micro-columnar fins with a size of 100 μm were etched in the 10 mm × 10 mm test surface in the center of the channel. The cross-section of each fin is made of a square with the size of 100 μm. Over the test surface area, the fins are arranged in parallel as shown in Fig. 4(a). There is a nucleated pore with a diameter of 60 μm at the center of each of the fins. The size of the pockets of each pore is 45 μm as seen in Fig. 4(a). The direction of the pockets is toward the outlet; the back is toward the inlet.

During the experiment, the working fluid enters the channel through the inlet hole and flows in the divergent area until it reaches to the fins over the test area. The heat transfer occurs between the working fluid and fins as well as the channel walls, and then, the fluid leaves the test area and flows toward the convergence area of the channel. Finally, it leaves the channel through the outlet hole. The inlet and outlet holes are connected to the stainless-steel basis by the gasket seals as described in the previous section.

2.4. Working fluid

A non-conductive liquid, FC-72, with the boiling point of 56.6 °C at 1 atm was used. FC-72 is adopted in the present study because the physical properties and chemical properties of this fluid are very stable, and it is a non-toxic and non-flammable liquid. Hence, the working fluid does not cause a short circuit in the system in the case of fluid leakage. Thus, it is suitable for working liquid for electronic heat dissipation. The thermophysical properties of FC-72 as a function of temperature can be evaluated using the following relations [39]:

$$C_p\,(J/kg\,^\circ C) = 1014 + 1.554\,(T) \tag{1a}$$

$$k_f\,(W/m\,^\circ C) = 0.060 - 0.00011\,(T) \tag{1b}$$

$$\rho_f\,(kg/m^3) = 1740 - 2.61(T) \tag{1c}$$

$$P\,(Pa) = EXP(9.729 - (1562/(T)) \tag{1d}$$

where C_p, k_f, ρ_f, and P denote the specific thermal capacity, thermal conductivity, density and the boiling pressure of FC-72 respectively. T is the temperature in °C. The other thermophysical properties of FC-72 including latent heat of evaporation (h_{fg}), dynamic viscosity (μ), the density of FC-72 vapor (ρ_g) and the surface tension (σ) are reported in Table 1. In order to investigate the heat transfer performance under different physical properties, two saturation temperatures of 35 °C and 50 °C are adopted in the present study.

2.5. Experimental equipment and measuring instruments

A pressure sensor (Cole Parmer, model EJA110A) with the measuring range from 0 to 172.36 kPa was placed in the cavity of the experiment to measure the saturation pressure in the chamber. The maximum error of the sensor is ±0.065% of the maximum pressure drop, i.e. ±0.112 kPa, and the sensor output signal is 4–20 mA. The output signal is converted into a DC output signal with the range of 1–5 V by connecting to a 250 Ω standard resistor. Then, the pressure output is received and displayed by a data logger. A differential pressure gauge (Cole Parmer, model EW-68071-60) with the measuring range 0–172.369 kPa is used to measure the pressure difference between the inlet and outlet of the test area. The maximum error is ±0.25% of the maximum differential

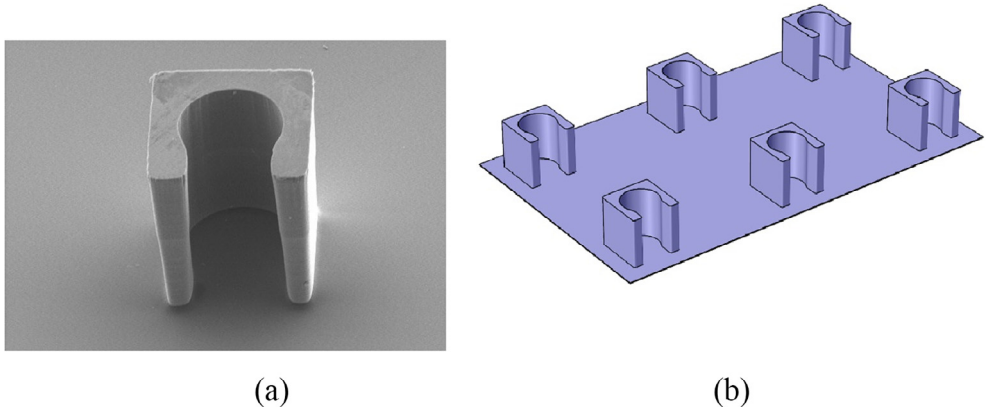

Fig. 4. The photo of etched fins, (a) the view of a single fin with the pore size of 60 μm and opening size of 45 μm, (b) schematic of the parallel arrangement of fins.

Table 1
The thermophysical properties of FC-72 at various saturated pressures [39].

P [kPa]	T [°C]	h_{fg} [J/kg]	$\mu \times 10^4$ [Pa × s]	ρ_g [kg/m^3]	σ [N/m]
23.5074	20	94368.5	6.86	3.484	0.0115
36.578	30	91820.3	6.011	5.231	0.01059
54.7155	40	89173.6	5.535	7.589	0.009708
67.12781	45	87788.8	5.091	9.136	0.009271
79.54013	50	86403.9	4.831	10.683	0.008838
90.43256	55	84969.8	4.608	12.738	0.008409
101.325	56.6	84510.9	4.537	13.396	0.008273
112.3694	60	83535.7	4.388	14.793	0.7985

pressure or ±0.43 kPa, and the output signal is a DC 1–5 V that is logged using a data logger.

The flow rate of FC-72 is monitored by a float ball type flowmeter (AALBORG, model P31A4-BAO/044-40-ST). When the working fluid is water, the flow range is 0–150 ml/min; the maximum error is ± 1.5% of the maximum flow, i.e., ±2.25 ml/min. Since this study uses FC-72 as the working fluid, the flow rate correction along with the calibration process is performed for the float-type flowmeter before the start of the experiment. The corrected error is within ±6%.

The micro gear-pump used in this experiment consists of a controller and a micro gear-pump head. The controller (RZ-75211-10) and micro gear-pump head (RZ-07002-26) are manufactured by Cole Parmer. The controller is mainly used to adjust the motor speed, and the output flow rate is adjusted by changing the motor speed.

The thermocouples for measuring temperature are Sheathed T-type (Omega) thermocouples with an outer probe diameter of 0.5 mm. The factory accuracy of the thermocouples is ±0.5 °C. Three thermocouples are used to measure the fluid inlet temperature of the microchannel. One of the thermocouples is placed inside the fluid flow, and two other thermocouples are placed at the inlet tube surfaces.

Five thermocouples with the wire diameter 0.08 mm are embedded in the drilled holes below the test surface area as depicted in Fig. 3(a). The thermocouples are utilized to measure the test surface temperature along the flow direction in the test area from the inlet toward the outlet. One of these five thermocouples is placed exactly at the center of the test surface to record the temperature of the test surface area. To obtain a more accurate temperature measurement, all thermocouples were temperature-corrected before commencing the experiments.

An AC transformer with a maximum output power of 100 W is used to power up the thin soft heater, and the output voltage and current of the transformer are adjusted to control the heat generation in the heater and consequently the surface heat flux of the wafer. A vacuum pump (ULVAC, model is GVD-050A) with the maximum vacuum pressure 5×10^{-4} Torr is utilized at the beginning of experiments. The vacuum procedure is performed to evacuate the non-condensable gas, impurities, and water in the cavity. This procedure ensures that the cavity is in a vacuum state, and the working fluid is filled according to the experiment.

The signals measured by each sensor in the experiment were transmitted to the data logger (model 34970A) to be captured and monitored. Later, the captured data was transmitted to a computer for data analysis. When performing a heat transfer experiment, it is necessary to capture and record the working fluid bubbles and gas formation at the test surface. The image capturing is mainly performed by a digital monocular camera (Nikon, model D5100) with an external magnification of 1:9 microscope and a minimum working distance of 18.5 mm. The photographic equipment was used to take and record the boiling process in the experiment. A light source part (Luminar Ace, model LA-60Me-R) as an auxiliary device with an input voltage of 100 VAC and a 60 W metal halide lamp with an average brightness of 2,500,000 lux is also utilized. In the structure of the surface and the measurement of the aperture size, a microscope (FS-230 T) with the magnification range of 1–230 times and the capability of five-segment zoom is used. This capturing setup can display the structure of the surface and capture adequate pictures.

Two liquid flow filters are utilized in the present experiment. A filter is installed in the circulation line at the outlet of the condensing plate heat exchanger as depicted in Fig. 1. The filter is a multilayer 10 μm grid. After installing the grid, the metal residue and impurities in the circulation line can be filtered to ensure the purity of the liquid flowing in the micro gear-pump. A 5 μm grid filter is also placed after the flowmeter before the liquid flows in the test area to ensure that impurities do not flow into the test area and cause microchannel blockage.

3. Analysis of experimental data

The present experiment tends to study the forced convection-boiling heat transfer behavior of the liquid coolant. Hence, in each experiment, the flow rate is kept constant, and the heat flux is increased to monitor and analyze the heat transfer behavior of the channel heat sink in forced convection boiling. The following relations are employed for heat transfer analysis.

The heat flux calculation of the test surface is obtained by multiplying the input voltage by the input current and dividing by the projected area as:

$$q'' = (Q - Q_{loss})/A_p = (V \times I - Q_{loss})/A_p \tag{2}$$

where Q is the input power (W), Q_{loss} is the test area inlet and outlet heat loss (W), V is the input voltage (V), I is the input current (A), q'' is the surface heat flux, and A_p is the projected area. Here, Q_{loss} is accounted for 2–8% of the total input heat.

The test surface wall temperature T_w is calculated by measuring the average temperature of the five-point wall temperatures on the wafer, and then correcting the surface temperature by the Fourier heat conduction law as:

$$T_{wall} = (T_{w1} + T_{w2} + T_{w3} + T_{w4} + T_{w5})/5 - q'' \times l/k \tag{3}$$

where $T_{w1\sim5}$ are the wall surface temperatures of the test surface distributed along the flow field, l is the distance from the temperature measurement position to the test surface (about 230 μm), k is the heat transfer coefficient of the wafer (about 1.24×10^{-2} W/mK).

The saturation temperature, T_{sat}, in the test area is obtained by the evaluation of the average pressure at the inlet and outlet of the test area in the circulation line, as:

$$T_{sat} = f(P_{av}) \tag{4}$$

where P_{av} is evaluated as $(P_i + P_o)/2$ in which P_i is the inlet pressure, and P_o is the outlet pressure of the circulation line. Here, f denotes the function or table converting the saturated pressure to the

saturated temperature. The corresponding saturated temperature of each pressure was reported in Table 1. The inlet temperature of the wafer device is evaluated as the average temperature of the inlet measured using three inlet thermocouples as:

$$T_{in} = (T_{i1} + T_{i2} + T_{i3})/3 \tag{5}$$

where T_i is the inlet temperature of each thermocouple. The convection-boiling heat transfer coefficient (h) of performance is calculated by dividing the heat flux by the wafer surface temperature minus the fluid inlet temperature (ΔT_{wi}) as:

$$h = q''/(T_{wall} - T_{in}) \tag{6}$$

The vapor quality of the outlet can be calculated from the known mass flow rate and the net input heat, as:

$$x_e = \frac{(Q - Q_{loss}) - \dot{m}c_p(T_{sat} - T_{in})}{\dot{m}h_{fg}} \tag{7}$$

where $\dot{m}$ is the mass flow rate in the test area, and h_{fg} is the latent heat of evaporation. The mass velocity (G) of the microchannel is calculated by dividing the working fluid mass flow rate ($\dot{m}$) by the channel inlet cross-sectional area (A_c) as:

$$G = \dot{m}/A_c \tag{8}$$

4. Results and discussion

In this section, the effect of various experimental parameters on the heat performance of the micro-three-dimensional fins is studied. The phase change and the initial boiling superheat are discussed. In this experiment, dielectric liquid FC-72 is used as the cooling fluid, which flows through the micro-column pore structure test surface. The experiments are performed for the saturation temperatures of 35 °C and 50 °C. During the experiment, the liquid flow rate was adjusted to 6–30 ml/min and the mass velocity was 94–275 kg/m^2 s, flowing through the microchannel with a fixed channel height of 100 μm, and the microchannel width of 10 mm. The minimum heating condition of the test surface is 1 W, and the maximum heating amount is the upper limit of the test surface overheat (>100 °C) or the test surface inlet and outlet pressure difference (>15 kPa).

Fig. 5 and shows the heat flux and surface superheat temperature difference at a saturation temperature of 50 °C for various mass fluxes in the range of 94–275 kg/m^2 s. Fig. 6 depicts the heat

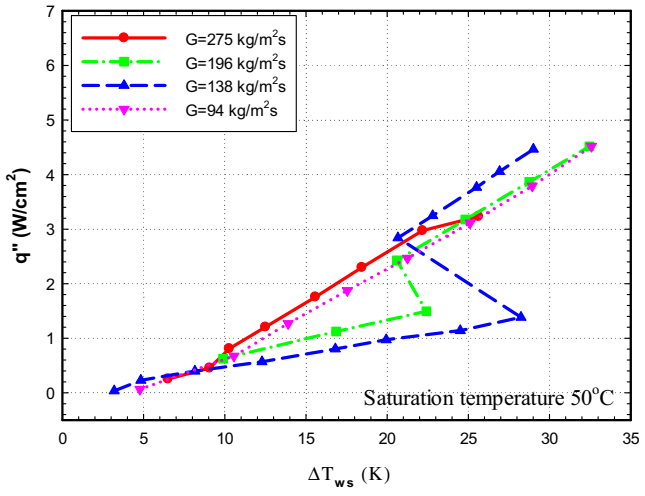

Fig. 5. The temperature difference of the test-surface at the saturation temperature of 50 °C.

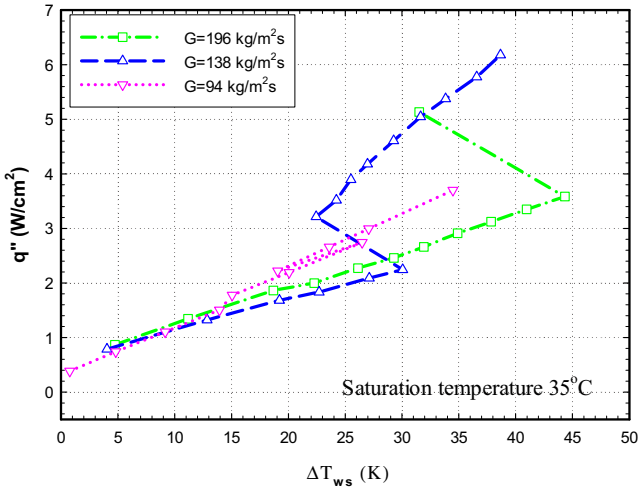

Fig. 6. The temperature difference of the test-surface at the saturation temperature of 35 °C.

flux as a function of surface temperature difference at three mass velocities of 94, 138 and 196 kg/m^2 s when the saturation temperature is 35 °C.

Figs. 5 and 6 show when the mass velocity is low, 94 kg/m^2 s, a small rise in the heat flux would result in a large increase of the temperature surface in both cases of the saturation temperatures of 50 °C and 35 °C. In the case of the boiling saturation temperature of 50 °C, the boiling phase occurs at a very low heat flux of q'' = 0.67 W/cm^2 corresponding to the very low-temperature difference of 4.7 °C. In this case, the transient to boiling condition occurs very smoothly. In the case of the saturation temperature of 35 °C, the change phase occurs at a higher heat flux of q'' = 1.7 W/cm^2 which corresponds to a higher test surface difference of 15 °C. However, when the heat flux is in the range of q'' = 2–3 W/cm^2, the test surface temperature fluctuates in the range of 19–27 °C. In the case of FC-72 with the saturation temperature of 50 °C, there is a monotone increase of the temperature surface from 17 to 22 °C when the heat flux rises from 2 to 3 W/cm^2. This region can be of interest for practical using of FC-72 as a working fluid with the low saturation temperature of 35 °C.

Fig. 5 indicates that the increase of the mass velocity to 138 kg/m^2 s increases the superheat temperature difference, but the further increase of the mass velocity to 275 kg/m^2 s reduces the superheat temperature difference. Fig. 5 also shows when the mass velocity is 138 kg/m^2 s, at low heat flux (≦1.38 W/cm^2), the heat transfer mechanism in this region is mainly single-flow heat transfer, and the surface-superheat increases linearly with the increase of heat flux. As the heat flux increases, the fin surface and the working fluid get hot, and the liquid begins to nucleate and boil at the downstream of the fin. The surface-superheat (ΔT) is 28.2 °C at the initial boiling. At this time, the heat transfer mechanism is convection boiling, and the surface-superheat temperature increases with the increase of the heat flux.

When the mass flux increases to 196 kg/m^2 s, the single-phase flow and heat transfer mechanism is consistent with 138 kg/m^2 s in both cases of 35 and 50 °C saturation temperatures. Considering the high heat flux rate of q'' = 3 W/cm^2, almost all of the flows are in boiling conditions. In these cases, the surface temperature differences for the mass flowrates of 94, 138, 196 and 275 kg/m^2 s are 22.5, 25, 22 and 25, respectively when the saturation temperature is 50 °C. Similarly, in the same case but the saturation temperature of 35 °C, the test surface temperature differences are 35, 24 and 27 °C for the mass flowrates of 94, 138, and 196 275 kg/m^2 s, respectively. As seen, the superheat temperature for the saturation

temperature of 35 °C is higher than the case of 50 °C. This difference is mainly due to the difference in the thermophysical properties of FC-72 at these two temperatures. For instance, the surface tension of FC-72 at 35 °C is 14.8% higher than that of 50 °C.

Figs. 7 and 8 are the graph of the heat transfer coefficient corresponding to the vapor quality of the experiments for two cases of the saturation temperatures of 50 °C and 35 °C, respectively. These figures show that the increase of the convective heat transfer corresponds to the increase of the bubble generation and the vapor quality of the outlet. Generally, the increase of the mass velocity reduces the vapor quality at the outlet and increases the convective heat transfer coefficient at the surface. The heat transfer coefficient ranges from 1410 to 2153.2 W/m^2 K, and the heat transfer mechanism in this region is mainly convection boiling mechanism. The trend of the convection coefficient is in agreement with the literature [10–14]. It should be noted that the vapor quality is calculated at the portion of the inlet mass, which transforms into vapor. Hence, as the inlet mass velocity increases, a smaller portion of the inlet mass is required to go through the change phase to absorb a fixed amount of the test-surface heat flux.

Fig. 9 depicts the flow and boiling phenomenon in the microchannel when the mass velocity is fixed at 94 kg/m^2 s. In the case of low heat flux of 0.67 W/cm^2, the initial boiling first occurs in the back part of the channel surface, and the boiling gas flows to the upstream direction of the channel only in a portion of the channel surface area. The vapor around the fins forms a continuous vapor area, which moves toward the outlet of the channel. As the heat flux increases to 1.26 (Fig. 9(b)) and 1.87 W/cm^2 (Fig. 9(c)), the boiling develops to the upstream and tends to cover more areas along the downstream of the channel surface. In this case, the vapor quality reaches to 0.309 and 0.427 corresponding to q″ = 1.26 W/cm^2 and q″ = 1.87 W/cm^2, respectively. In Fig. 9(a)–(f) the traces of the liquid flow between the fins is obvious. However, by further increase of the heat flux, the boiling phenomenon spreads toward the downstream and the vapor quality at the outlet increases. In the case of low heat flux, the regime of the boiling flow is in the form of bubbly flow, and by the increase of the heat flux, the regime of the boiling flow changes to the slug flow. In Fig. 9(g), the outlet is almost dry and only in few spots very small traces of the films of the liquid can be observed. The trend of the boiling behavior of Fig. 9 agrees with force convection boiling behavior in a structured microchannel as reported in [29].

In this experiment, the differential pressure gauge device is used to measure the pressure difference before and after testing

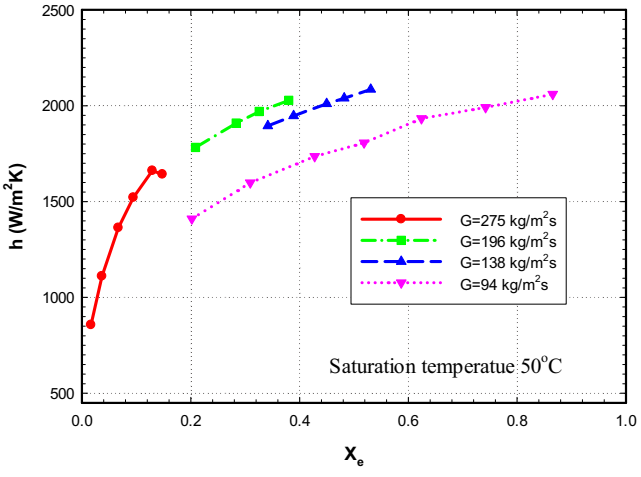

Fig. 7. The convective heat transfer coefficient as a function of the outlet vapor quality for various mass flow rates when the saturation temperature is 50 °C.

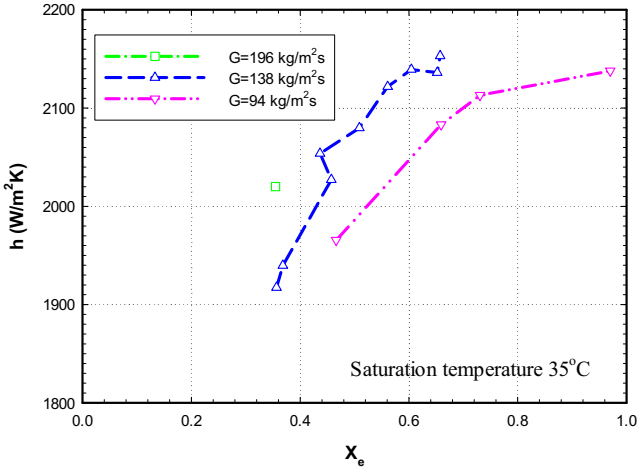

Fig. 8. The convective heat transfer coefficient as a function of the outlet vapor quality for various mass flow rates when the saturation temperature is 35 °C.

the microchannel. The relationship between the mass velocity and the pressure drop of different surfaces is plotted in Figs. 10 and 11 for two saturation temperatures of 50 °C and 35 °C, respectively.

Fig. 10 shows the pressure drop in the channel as a function of the surface heat flux for various mass velocities in the range of 94–275 kg/m^2 s. Figs. 10 and 11 reveal that the pressure-drop increases by the increase of the mass velocity when the coolant is still in a single liquid phase. Moreover, the increase of the heat flux reduces the pressure-drop when there is no boiling, and the coolant is solely in the liquid phase. The reduction of the pressure drop, in this case, is due to the decrease of the dynamic viscosity of the coolant by the increase of the liquid temperature (the increase of heat flux). When the heat flux continues to increase, the initial boiling occurs, and the heat transfer mechanism changes to a two-phase boiling mechanism. At this time, the heat flux is increased, and the channel pressure-drop is significantly increased. Indeed, the bubbles in the channel cause the liquid blockage. Moreover, the volume of the vapor is significantly higher than the liquid, and hence, more volume of fluid should be passed through the channel resulting in a significant pressure drop across the channel. In the case of very low mass velocity of 94 kg/m^2 s, Fig. 10 shows a monotonic increase of pressure drop by the increase of heat flux. In fact, in this case, the boiling occurs at the very small heat fluxes.

For the same case, Fig. 11 depicts that there is a significant region for the heat flux range of 0–4 W/m^2 K in which the liquid FC-72 gets superheat before commencing of boiling heat transfer when the saturation temperature is 35 °C. Figs. 10 and 11 indicate a monotonic increasing trend of pressure-drop by the increase of the heat flux after the boiling pressure jump. This trend of boiling behavior is similar to the literature for convective boiling cooling in structured microchannels [29].

5. Conclusion

The effect of the mass velocity and heat flux of the working fluid FC-72 on the heat transfer performance was investigated experimentally. The channel has a total length of 1 cm, a width of 1 cm and a height of 100 μm. The test surface is an etched surface with a columnar fin height of 100 μm. The fins are distributed in a parallel arrangement, and the working fluid inlet temperature is controlled at 35 and 50 °C. The flow rate is studied in the range of 94–275 kg/m^2 s, the heat flux range is adopted as 1–6 W/cm^2. The experimental results are reported for the convective heat transfer

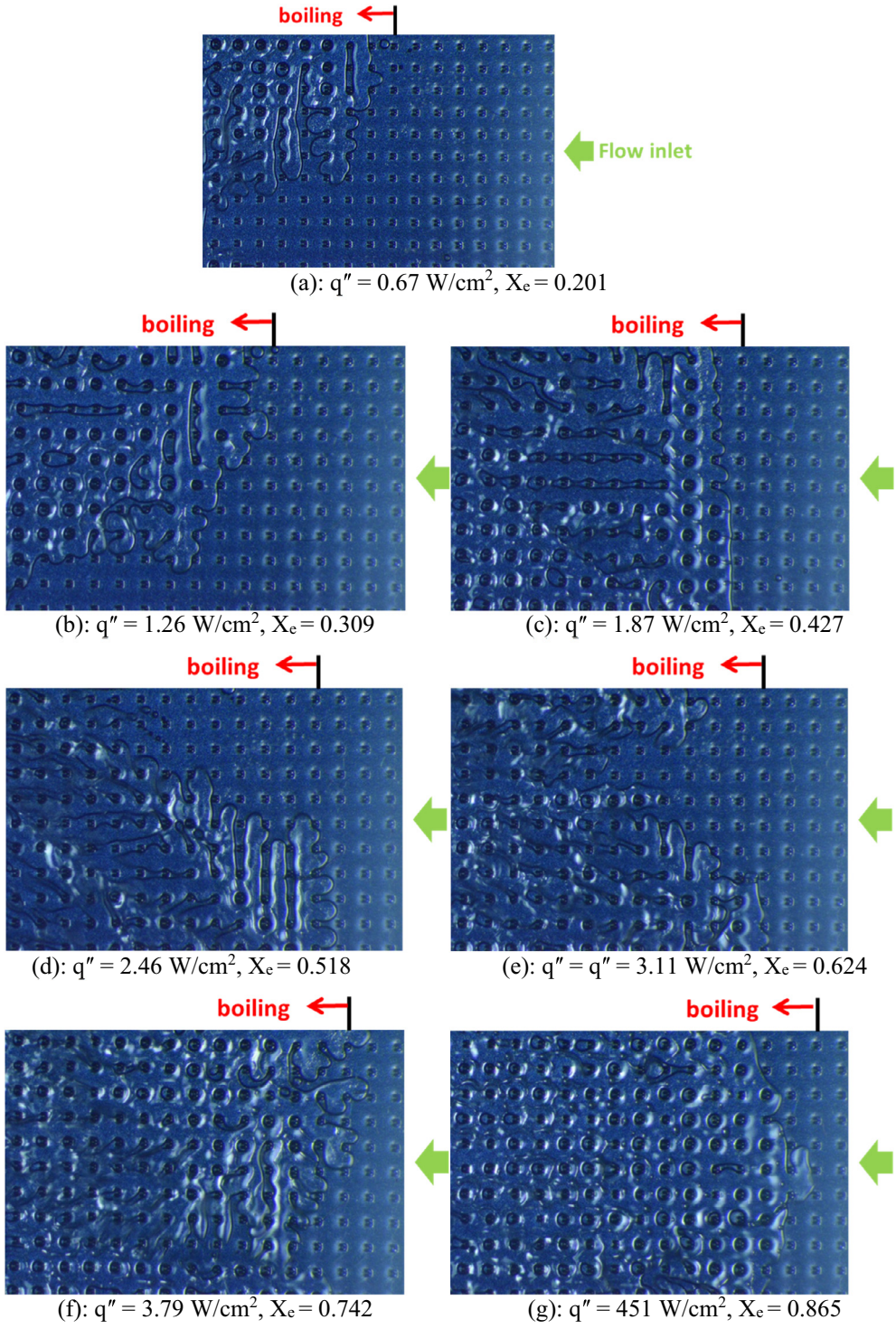

Fig. 9. Heat flux, outlet vapor quality and flow field change diagram of the test surface at 50 °C.

coefficient, the vapor quality of the channel outlet, and pressure drop across the channel. The photographs of the boiling behavior of FC-72 over the fins are also reported. The main outcomes of the present study can be summarized as follows:

1. At a saturation temperature of 50 °C, when the mass velocity is 94–138 kg/m^2 s, the superheat required for initial boiling increases with the increase of mass velocity; but at high flow rates (138–275 kg/m^2 s) the superheat temperature shows a decreasing trend of behavior.
2. Generally, the pressure drop in the liquid phase increases by the increase of the mass velocity in the channel. The increase of heat flux would smoothly decrease the pressure-drop due to the decrease of FC-72 dynamic viscosity by the increase of its temperature. However, in the case of boiling convection, the increase of heat flux significantly increases the pressure drop. For example, in the case of a mass flow rate of 196 kg/m^2 s and saturation temperature 50 °C, the increase of the heat flux from 0 to 3 W/m^2 K reduces the pressure-drop from 5.8 kPa to

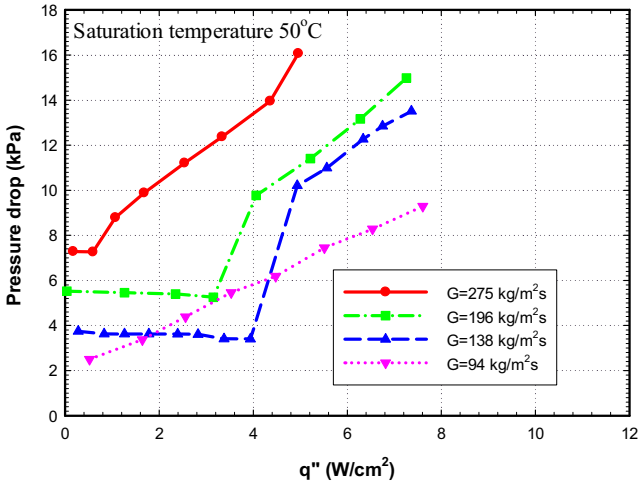

Fig. 10. The channel pressure-drop as a function of heat flux for various values of mass velocity at the saturated temperature of 50 °C.

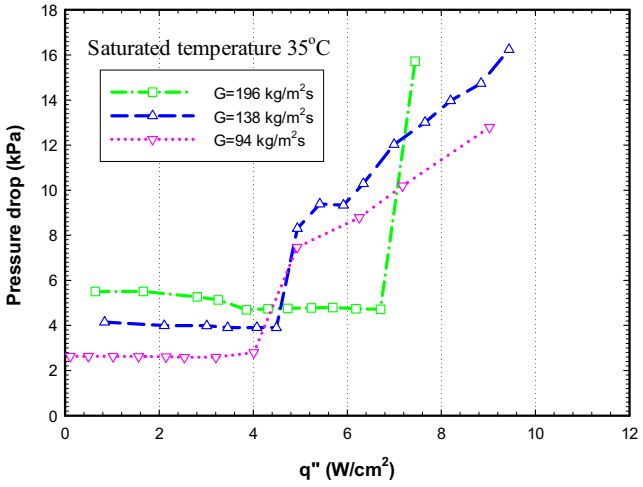

Fig. 11. The channel pressure-drop as a function of heat flux for various values of mass velocity at the saturated temperature of 35 °C.

5.5 kPa in the single-phase flow. However, the increase of the heat flux from 3 to 6 W/m^2 K would dramatically increase the pressure-drop from 5.5 kPa to 13 kPa.

3. The change in the saturated temperature from 50 °C to 35 °C would generally postpone the boiling phenomenon and increase the superheat temperature.
4. The flow in the microchannels of this study is mainly bubbly flow when the heat flux is low. The increase of the heat flux also changes the boiling flow regime from the bubbly flow to slug flow.
5. In the present study, the parallel fin arrangement with a fixed inner pore size of 60 μm and the opening of 45 μm is studied. However, it seems that the change in the size of pores and changing the structure of the fin arrangements to a segregated array can change the flow behavior and pressure-drop in the channel. The results of the present study show that the change in the saturation temperature of the experiment induces significant changes in the superheat temperature of the test surface. This difference was due to the difference between the working temperatures and consequently the change in the thermophysical properties of FC-72. Hence, a study of the thermal behavior of other dielectric fluids can be subject of future studies.

Conflict of interest

The authors declared that there is no conflict of interest.

Acknowledgements

The authors appreciate the financial support from Ministry of Science and Technology, Taiwan, under grant number MOST 101-2221-E-027-044-MY2. The authors also appreciate the financial support by the "Research Center of Energy Conservation for New Generation of Residential, Commercial, and Industrial Sectors" from The Featured Areas Research Center Program within the framework of the Higher Education Sprout Project by the Ministry of Education (MOE) in Taiwan.

References

[1] M.A. Ebadian, C.X. Lin, A review of high-heat-flux heat removal technologies, J. Heat Transfer 133 (11) (2011) 110801.
[2] IBM Power Systems Announce Overview, <http://www-03.ibm.com/systems/resources/systems_power_news_announcement_20080408_annc.pdf>, 2008.
[3] L. Campbell, M. Ellsworth, Back to the future with a liquid cooled supercomputer, Electronics Cooling (2005).
[4] F. Alfieri, M.K. Tiwari, I. Zinovik, D. Poulikakos, T. Brunschwiler, B. Michel, 3D integrated water cooling of a composite multilayer stack of chips, in: 14th International Heat Transfer Conference, vol. 3, 2010, pp. 565–574.
[5] A. Finch, E. Ballew, Direct Spray Cooling and System-level Comparisons, <http://www.electronics-cooling.com>, 2009.
[6] M. Lie, J.H. Ke, W.R. Chang, T.C. Cheng, T.F. Lin, Saturated flow boiling heat transfer and associated bubble characteristics of FC-72 on a heated micro-pin-finned silicon chip, Int. J. Heat Mass Transfer 50 (2007) 3862–3876.
[7] C.T. Yeh, A Study of Enhanced Heat Transfer in Micro Heat Exchanger for Liquid Cooling Ph.D Dissertation (in Chinese), Department of Mechanical Engineering, National Central University, Taiwan, 2008.
[8] W. Escher, B. Michel, D. Poulikakos, A novel high performance, ultra thin heat sink for electronics, Int. J. Heat Fluid Flow 31 (2010) 586–598.
[9] W. Escher, B. Michel, D. Poulikakos, Experimental investigation of an ultrathin manifold microchannel heat sink for liquid-cooled chips, Proc. ASME-JSME Therm. Eng. Summer Heat Transfer Conf. 132 (2010).
[10] T.H. Hwang, S.C. Yao, Cross flow heat transfer in tube bundles at low Reynolds numbers, J. Heat Transfer 108 (1986) 697–700.
[11] J.T. Hsu, A Parametric Study of Boiling Heat Transfer in a Horizontal Tube Bundle Ph.D. Dissertation, University of Wisconsin-Milwaukee, Milwaukee, USA, 1987.
[12] M.K. Jensen, J.T. Hsu, A parametric study of boiling heat transfer in a horizontal tube bundle, J. Heat Transfer 110 (1988) 976–981.
[13] A. Gupta, J.S. Saini, H.K. Varma, Boiling heat transfer in small horizontal tube bundles at low cross-flow velocities, Int. J. Heat Mass Transfer 38 (4) (1995) 599–605.
[14] A. Gupta, Enhancement of boiling heat transfer in a 5 x 3 tube bundle, Int. J. Heat Mass Transfer 48 (2005) 3763–3772.
[15] M.R. Hajmohammadi, P. Alipour, H. Parsa, Microfluidic effects on the heat transfer enhancement and optimal design of microchannels heat sinks, Int. J. Heat Mass Transfer 126 (2018) 808–815.
[16] J. Wang, J.M. Li, Y. Hwang, Modeling of film condensation flow in oval microchannels, Int. J. Heat Mass Transfer 126 (2018) 1194–1205.
[17] L. Zhou, S. Zhou, X. Du, Y. Yang, Heat transfer characteristics of a binary thin liquid film in a microchannel with constant heat flux boundary condition, Int. J. Therm. Sci. 134 (2018) 612–621.
[18] L. Gao, S.H. Bhavnani, Experimental study of augmented flow boiling in a dielectric fluid due to backward and forward facing stepped microchannels, Int. J. Heat Mass Transfer 124 (2018) 484–490.
[19] I. Monsivais, J.J. Lizardi, F. Méndez, Conjugate thermal creep flow in a thin microchannel, Int. J. Therm. Sci. 124 (2018) 227–239.
[20] A. Ferrari, M. Magnini, J.R. Thome, Numerical analysis of slug flow boiling in square microchannels, Int. J. Heat Mass Transfer 123 (2018) 928–944.
[21] R.K. Gouda, M. Pathak, M.K. Khan, Pool boiling heat transfer enhancement with segmented finned microchannels structured surface, Int. J. Heat Mass Transfer 127 (2018) 39–50.
[22] H.J. Kwak, J.H. Kim, B.S. Myung, M.H. Kim, D.E. Kim, Behavior of pool boiling heat transfer and critical heat flux on high aspect-ratio microchannels, Int. J. Therm. Sci. 125 (2018) 111–120.
[23] S. Hong, Y. Tang, S. Wang, Investigation on critical heat flux of flow boiling in parallel microchannels with large aspect ratio: experimental and theoretical analysis, Int. J. Heat Mass Transfer 127 (2018) 55–66.
[24] K. Nomura, H. Kumano, Experimental study on flow and heat transfer characteristics of oil-in-water emulsions in microchannels, Int. J. Heat Mass Transfer 116 (2018) 1026–1035.
[25] Q. Esmaili, A.A. Ranjbar, S. Porkhial, Experimental analysis of heat transfer in ribbed microchannel, Int. J. Therm. Sci. 130 (2018) 140–147.

[26] F.B.A. Hasis, P.M. Krishna, G.P. Aravind, M. Deepu, S.R. Shine, Thermo hydraulic performance analysis of twisted sinusoidal wavy microchannels, Int. J. Therm. Sci. 128 (2018) 124–136.
[27] X.J. Wei, Y. Joshi, Stacked microchannel heat sinks for liquid cooling of microelectronic components, J. Electron. Packag. 126 (2004) 60–66.
[28] X.J. Wei, Y. Joshi, M.K. Patterson, Experimental and numerical study of a stacked microchannel heat sink for liquid cooling of microelectronic devices, J. Heat Transfer 129 (2007) 1432–1444.
[29] S.S. Hsieh, C.Y. Lin, Subcooled convective boiling in structured surface microchannels, J. Micromech. Microeng. 20 (2010) 015027.
[30] S. Novianto, R. Koestoer, A.S. Pamitran, Heat transfer coefficient of near boiling single phase flow with propane in horizontal circular micro channel, IOP Conference Series: Earth and Environmental Science, vol. 105, IOP Publishing, 2018, p. 012005, 1.
[31] S. Korniliou, C. Mackenzie-Dover, S. Harmand, G. Duursma, J.R.E. Christy, J.G. Terry, A.J. Walton, K. Sefiane, Local wall temperature mapping during flow boiling in a transparent microchannel, Int. J. Therm. Sci. 135 (2019) 344–361.
[32] J. Mathew, P.S. Lee, T. Wu, C.R. Yap, Experimental study of flow boiling in a hybrid microchannel-microgap heat sink, Int. J. Heat Mass Transfer 135 (2019) 1167–1191.
[33] L. Yin, P. Jiang, R. Xu, H. Hu, L. Jia, Heat transfer and pressure drop characteristics of water flow boiling in open microchannels, Int. J. Heat Mass Transfer 137 (2019) 204–215.
[34] S. Lee, V.S. Devahdhanush, I. Mudawar, Frequency analysis of pressure oscillations in large length-to-diameter two-phase micro-channel heat sinks, Int. J. Heat Mass Transfer 116 (2018) 273–291.
[35] A. Parahovnik, Y. Wang, Y. Peles, Transient local resolution of flow boiling in a microchannel with a streamlined pin fin, 16th Int. Conference on Nanochannels, Microchannels, and Minichannels, 2018, pp. V001T02A001–V001T02A001.
[36] X. Yu, C. Woodcock, Y. Wang, J. Plawsky, Y. Peles, Enhanced subcooled flow boiling heat transfer in microchannel with Piranha Pin Fin, J. Heat Transfer 139 (11) (2017) 112402.
[37] C. Woodcock, C. Ng'oma, M. Sweet, Y. Wang, Y. Peles, J. Plawsky, Ultra-high heat flux dissipation with Piranha Pin Fins, Int. J. Heat Mass Transfer 128 (2019) 504–515.
[38] S.M. Kim, I. Mudawar, Thermal design and operational limits of two-phase micro-channel heat sinks, Int. J. Heat Mass Transfer 106 (2017) 861–876.
[39] V.P. Carey, Liquid-Vapor Phase-Change Phenomena, Taylor and Francis, London, 1992.